Special Interest Group Meeting on Thermal Issues
Laboratory for Machine Tools and Production Engineering (WZL) of
RWTH Aachen, Germany, February 2020
www.euspen.eu

Deformation-based control of a thermo-mechanical system

Dennis Heck[1], Nic Dirkx[1], Wijnand Hoitinga[2], Johan Kunnen[1], Marc van de Wal[1]
[1]ASML, 5504 DR Veldhoven, The Netherlands
[2]Evalf, Burgwal 45, 2611 GG Delft, The Netherlands

dennis.heck@asml.com

Abstract
In this work, we introduce the concept of a Deformation-Based Controller (DBC) to improve the performance, in terms of thermal deformations, of a temperature controlled thermo-mechanical system subject to unpredictable thermal disturbances. In a traditional temperature controlled system, thermal actuators are used to control the temperature *at sensor locations* towards a desired setpoint. Since the temperature is not controlled in-between the sensor locations, there can arise thermal gradients in the system, which result in undesired thermal deformations in the whole system. DBC aims to reduce these thermal deformations while using only the existing thermal actuators and sensors, such that hardware changes are not required. Experiments with a system subject to unpredictable evaporation loads demonstrate that a significant reduction in thermal deformations is achieved, compared to a traditional temperature controller.

Control, Temperature, Deformation, Observer

1. Introduction

In many industrial high precision applications, such as electron microscopes and lithography machines, thermal specifications are continuously tightened to improve the performance in terms of accuracy and availability [1]. As a result, reducing temperature fluctuations and the resulting thermal deformations of components, often resulting from unpredictable and uncontrollable thermal disturbances, becomes highly important.

A reasonable thermal performance can often be achieved with a good thermal design and insulating or shielding of thermal loads. When thermal disturbances cannot be insulated completely, (multiple) thermal actuators (e.g. heaters) and (temperature) sensors can be added and combined with a temperature feedback controller (e.g. a PID-controller) to suppress the effect of the thermal disturbances by controlling the temperature to a desired setpoint. In this way, a satisfying thermal performance can be achieved, but *only at the sensor locations*. Thermal gradients might still exist between the sensor locations and these result in undesired thermal deformations, limiting the precision of optical elements [2, 3].

To reduce the thermal deformations, we propose to control these thermal deformations instead of the temperatures. In practice it is not always possible (volume restrictions) or desired (extra costs and complexity) to add extra sensors to measure deformations. Therefore, we focus on a 'software-only' solution, where only the existing thermal actuators and sensors are used. This means that the resulting Deformation-Based Controller (DBC) is based on a high accuracy thermo-mechanical model of the system to estimate the thermal deformations from measured temperatures and these deformations are controlled using the thermal actuators.

There are many challenges in designing such a DBC. These challenges include the design of a high order thermo-mechanical model (>10 000 states), the identification of physical model parameters (e.g. contact resistances and heat transfer coefficients) to improve the model accuracy, model order reduction to make control design feasible, disturbance modelling, Multiple Input-Multiple Output (MIMO) controller design and closed-loop controller order reduction to compute the model-based controller in real-time. The main contribution of this work is to provide a framework for DBC, illustrating the steps taken, and how the previously mentioned challenges can be overcome.

This abstract proceeds as follows. In Section 2, the physics of the considered thermo-mechanical system are explained. The DBC design steps and solutions to the previously mentioned challenges are explained in Section 3. Subsequently, Section 4 shows experimental results to illustrate the reduction in thermal deformations that can be obtained with DBC over a commonly used temperature controller. Finally, the conclusions and future work are described in Section 5.

2. System description

The system considered in this work consists of a 300 mm disk of 10 mm in height, with water cooling channels, as illustrated in Figure. 1. The top surface of this disk should remain as flat as possible. Due to the operation process of the machine, the top edge of the disk is irregularly wetted with water. To keep the top surface dry, the water is first extracted via small holes into an Edge Channel (EC), inside the edge of the disk, and then from the EC via several extraction holes at the bottom of the disk. A part of this water evaporates in the EC, thereby extracting up to 15 W of heat from the disk. As a result, the edge of the disk cools down (in the order of 100 mK) and this results in several nanometres of thermal deformations of the edge, affecting the flatness of the top of the disk. To compensate for the evaporative load, 12 segmented heaters are attached to the edge (covering the whole edge) and 12 sensors are attached (8 cm apart) to the bottom of the disk, below the EC, as illustrated in Figure 1. These heaters and sensors are available for control.

2.1. Thermo-mechanical model

A spatially discretized and parametrized thermo-mechanical finite element model of the system is created using Nutils [4].

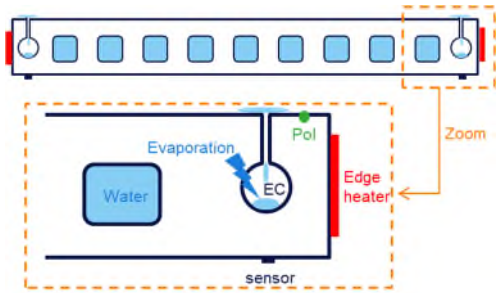

Figure 1. Impression of the cross section of the disk with cooling water, EC with evaporation load, edge heaters, temperature sensors and the Point of Interest (PoI) for DBC.

The resulting dynamics are described in descriptor state-space form as

$$\begin{aligned} E(p)\dot{T} &= A(p)T + B_1 u + B_2 w \\ y &= C_y T \\ d &= C_d T \end{aligned} \tag{1}$$

with $T \in \mathbb{R}^n$ the states (temperatures) of the full system, consisting of $n = 50\,000$ states, $u \in \mathbb{R}^{12}$ the heater power inputs, $w \in \mathbb{R}^{100}$ the evaporation loads in the EC, modelled over 100 segments, $y \in \mathbb{R}^{12}$ the temperatures measured by the sensors and $d \in \mathbb{R}^{100}$ the stacked deformations in x- and y-direction of 50 uniformly distributed points at the top edge of the disk (see Figure 2), also referred to as the Points of Interest (PoI). The matrices B_1 and B_2 are the input matrices of u and w, respectively, and C_y and C_d are the output matrices related to y and d, respectively. The capacity matrix $E(p)$ and conductivity matrix $A(p)$ depend linearly on the physical model parameters $p \in \mathbb{R}^{50}$, i.e.

$$E(p) = \sum_{i=1}^{50} p_i E_i\,, \qquad A(p) = \sum_{i=1}^{50} p_i A_i. \tag{2}$$

with E_i and A_i representing the structural contribution of parameter p_i, $i = 1,2,\ldots,50$, to E and A, respectively. The parameters p consist of the physical parameters of the disk (e.g. thermal masses, heat transfer coefficients, conductivities, water flow, etc.) and the dynamics of the heaters and sensors (modelled with a time constant). The uncertainty on the parameters is on average ~10 % due to production tolerances and variations in flows between different systems.

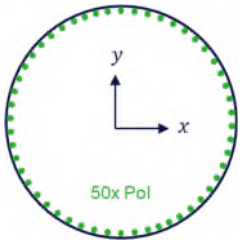

Figure 2. Top view of the disk with the 50 deformation nodes (PoI).

2.2. Characteristics of disturbance w

The evaporation disturbance $w_i \in \mathbb{R}_{\leq 0}$ of an element in w can be characterized by the illustration in Figure 3. The thermal evaporation load is present at ① when there is water in the EC segment and the local humidity is below 100 %. The load drops to zero when the humidity is 100 % or when all the water is extracted via the bottom holes or evaporated in the EC. The humidity reaching 100% could be a local effect ②, when the supply of dry air via the holes is blocked (due to the production process), or it could be a global effect ③ when the extraction flow is switched off (also due to the production process). The local effect, which causes the largest temperature gradients and disk deformations, occurs for each of the 100 segments at different time instances during production and is not known in advance.

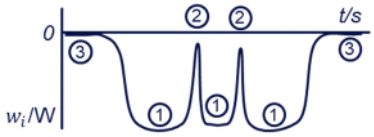

Figure 3. Impression of the repetitive disturbance characteristic w_i. At ① evaporation takes place, at ② the evaporation stops due to a blocked hole and at ③ the extraction flow (sucking dry air in the EC) is switched off.

3. Deformation-based control design

The goal of the DBC is to minimize the deformations d when the system is subject to the unmeasurable disturbance w, characterized in Section 2.2. The deformations cannot be measured directly. Instead, only the temperature measurements y are available. To estimate the deformations, an observer is used, as illustrated in Figure 4. The challenges involved in designing an accurate observer are discussed in Section 3.1. Thereafter, Section 3.2 discusses the design of the MIMO controller to minimize d, and Section 3.3 discusses how the observer and the MIMO controller can be combined and efficiently implemented on a control board.

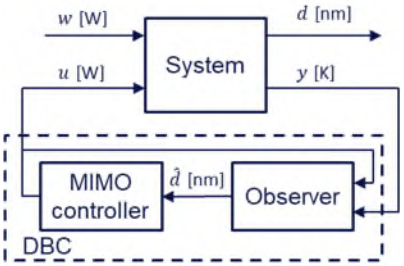

Figure 4. Block diagram of the DBC controller, consisting of an observer and a MIMO controller. The observer estimates d from the measurements y and the applied input u and the MIMO controller computes u to drive $\hat{d}$ to zero.

3.1. Observer design

The main challenge when designing an observer is to obtain an accurate thermo-mechanical model. For our system, the model structure in (1) is used as a basis. Due to the uncertainty on the model parameters p, an identification experiment is conducted using only u and y to accurately identify these parameters. When calibrating these parameters it is important that the input signal u results in a sufficiently high sensitivity of each parameter in the measured response and that the contribution to each parameter can be separately identified (limited correlation). We experienced for our system that the best results can be obtained when calibrating the parameters based on a measured Frequency Response Function (FRF) of the system (both magnitude and phase), rather than performing the calibration on a time-domain signal. The main reason is that time-domain signals for thermal systems are usually dominated by low frequency dynamics far below the desired bandwidth of the controller. To accurately measure the FRF, a standard system identification, e.g. using white noise- or multi-sine injection [5], is sufficient. Note that the same measured FRF is often already measured to tune a traditional temperature controller.

Using the measured FRF of the MIMO system, the parameters are calibrated following the optimization procedure illustrated in Figure 5. In this iterative optimization procedure, the gradient

of the FRF with respect to each parameter is used to determine the parameter update direction. This gradient is determined using the perturbation method [6], where, per iteration, for all 50 parameters the FRF of the model with one perturbed parameter is compared with the FRF of the unperturbed model. Per iteration this yields 50+1 computed model FRFs to be computed, which is computationally very expensive when using the full order model of (1) with 50 000 states. To speed up the process, we propose to use the parametric model-order reduction technique of [7], which is an extension of the commonly used Arnoldi reduction technique [8], to obtain a parametrized reduced order model (of 500 states) that needs to be computed only once, outside the iterative loop. The calibration of the 50 parameters of the 12x12 MIMO system takes only ten minutes using Matlab on a Lenovo P52 with Intel Xeon E-2176M processor.

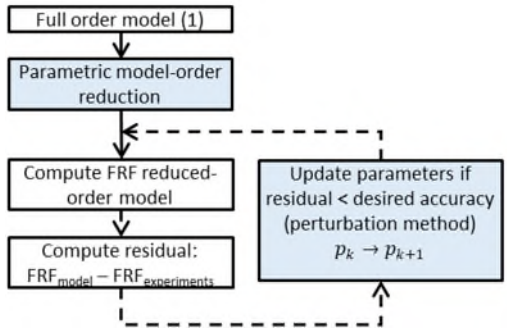

Figure 5. Outline parameter calibration procedure. The dashed arrows represent an iterative loop that stops when the desired accuracy is achieved.

The observer to estimate d is a Kalman filter [9] based on a reduced order version (500 states) of the model (1), obtained using the reduction method of [7]. Since the disturbance w cannot be modelled by white noise (one of the requirements for using a Kalman filter), the system dynamics are augmented with a dynamical model of the disturbance to map a white noise input $w_{white} \in \mathbb{R}^{100}$ to w used in (1), i.e.

$$\begin{aligned} \dot{x}_w &= A_w\, x_w + B_w\, w_{white}, \\ w &= C_w x_w, \end{aligned} \tag{3}$$

with $x_w \in \mathbb{R}^{100}$. An integrator model is considered sufficient for the problem at hand, so $A_w = O$ and $B_w = C_w = I$. The augmented Kalman filter is then expressed by

$$\begin{aligned} \begin{bmatrix} \dot{\hat{T}} \\ \dot{x}_w \end{bmatrix} &= \begin{bmatrix} \hat{A} & \hat{B}_2 C_w \\ O & A_w \end{bmatrix} \begin{bmatrix} \hat{T} \\ x_w \end{bmatrix} + \begin{bmatrix} \hat{B}_1 \\ 0 \end{bmatrix} u + L\,(y - \hat{y}), \\ \hat{y} &= \begin{bmatrix} \hat{C}_y & O \end{bmatrix} \begin{bmatrix} \hat{T} \\ x_w \end{bmatrix}, \\ \hat{d} &= \begin{bmatrix} \hat{C}_d & O \end{bmatrix} \begin{bmatrix} \hat{T} \\ x_w \end{bmatrix}, \end{aligned} \tag{4}$$

with $\hat{(\ )}$ an estimate of the actual matrices (obtained after parameter calibration) and signals. The Kalman gain L is obtained by solving a Riccati equation with a disturbance covariance matrix Q_w and measurement noise covariance matrix $R = \gamma_r I$, $\gamma_r = (10^{-4})^2$ K². Due to the nature of the disturbance (in particular effect ① in Figure 2), w is strongly correlated. The correlation of w is included in Q_w as illustrated by the matrix structure in Figure 6.

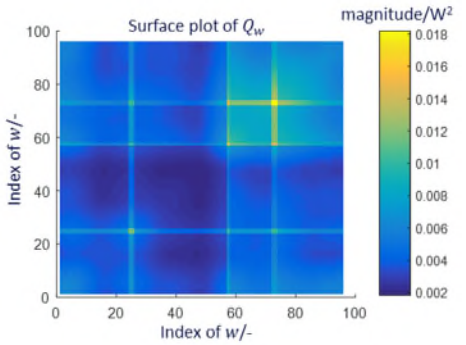

Figure 6. Structure of the covariance matrix Q_w, illustrating the correlation of elements in w (an uncorrelated signal is represented by a diagonal structure). The lines standing out are related to locations where water is extracted from the EC at the bottom of the disk. Here, the evaporative load is larger compared to the other EC elements.

3.2. Feedback control design

Due to the large number of input signals (12 heater powers) and performance variables (100 deformations), manually designing and tuning a feedback controller is too cumbersome. Instead, a Linear-Quadratic Regulator (LQR) [9] is used as MIMO controller. LQR is a state-feedback controller that computes the input u based on the estimated states $\hat{T}$ via

$$u = -K\hat{d} = -KC_y\hat{T}, \tag{5}$$

with $K \in \mathbb{R}^{12\times 500}$, and $\hat{T}$ the estimate state from the observer (4). The matrix K follows from solving a Riccati equation to minimize the following cost function

$$J = \int_{t=0}^{\infty} \left(\hat{d}^T Q_d \hat{d} + u^T u\right) dt, \tag{6}$$

which is modified to drive $\hat{d}$ to zero, instead of $\hat{T}$. Here, $Q_d = \gamma_d I$, γ_d being a positive scalar to tune the aggressiveness of the controller.

3.3. DBC implementation

The total DBC consists of the observer (4) and the controller (5), indicted by the dashed box in Figure 3, and has 500 states. This controller is too expensive to compute in real-time. Therefore, the DBC controller with 12 *controller* inputs y and 12 *controller* outputs u is reduced to only 100 states using a closed-loop model order reduction technique (see [10, 11, 12]).

4. Experimental results

The DBC of Section 3 is implemented on the experimental system described in Section 2 and the estimated deformations are compared to the estimated deformations obtained when using a standard PID temperature controller $u = \left(K_p + K_d s + \frac{K_I}{s}\right)(y_{set} - y)$, where s is the Laplace variable, y_{set} is the temperature setpoint and K_p, K_d and K_I are the proportional, derivative and integral gains, respectively. Both controllers were tuned for maximal performance, with similar robustness margins.

During both experiments, the controller was implemented with a 200 Hz sampling frequency. The Kalman filter was implemented in parallel to estimate the deformations in real-time during both experiments. The x-component of these estimated deformations is shown in Figure 7 (the y-component shows similar results).

The left plot shows the deformations when using the temperature controller. The temperature error $y_{set} - y$ < 5 mK throughout the whole experiment, but because the temperature gradient in-between the sensor locations is not controlled, this

results in a too large thermal deformation for the specific process in the lithography machine.

The right plot of Figure 7 shows that with DBC the deformations are suppressed to 40 % compared to the temperature controller, which is considered a huge performance gain for a software solution. Finally, note that with DBC not all deformations can be controlled to zero, because the system is underactuated (nr. of actuators << nr. deformations to control), but the average can be steered to zero.

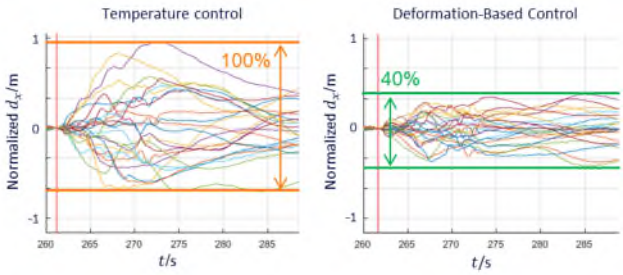

Figure 7. Real-time estimated deformations (x-component, normalized) of the 50 points at the top edge of the disk under closed-loop temperature control (left) and DBC (right). With DBC, the deformations are reduced to 40 %.

5. Conclusion and recommendations

In this work, we have shown for a temperature controlled thermo-mechanical system subject to unpredictable thermal disturbances that the performance, in terms of thermal deformations, can be improved significantly with a deformation-based controller. The advantage of the DBC controller is that it uses the same thermal actuators and sensors as the temperature controller, so no hardware changes are required. We have given a framework for the DBC and illustrated how to use parameter calibration, based on the measured FRF of the system, to obtain a high accuracy thermo-mechanical model, how to include disturbance information in the observer and how to design a MIMO controller to minimize the thermal deformations. Finally, we have demonstrated on an experimental system with unpredictable evaporation disturbances a performance improvement of 60 %, in terms of thermal deformations, over a standard temperature controller.

Future work focusses on developments towards an efficiently automated calibration and tuning of the DBC to be robust for variations in dynamics and disturbance loads between different systems.

References

[1] DSPE Mikroniek 2019 Vol 59 Issue 2 Eindhoven, the Netherlands

[2] Bikcora C, Weiland S and Coene W M J 2014 Thermal deformation prediction in reticles for extreme ultraviolet lithography based on a measurement-dependent low-order model *IEEE Tr. on Semiconductor Manufacturing* 27(1) p 104–117

[3] Habets M, Merks R, Weiland S and Coene W 2015 A multiphysics modelling approach for thermal aberration prediction and control in extreme ultraviolet lithography *Imaging and Applied Optics* p AOM4B.2, Washington D.C., USA

[4] nutils.org/en/latest

[5] Pintelon R and Schoukens J 2012 System identification: A frequency domain approach *Wiley-IEEE Press* 2nd edition

[6] Spall J C 1992 Multivariate stochastic approximation using simultaneous perturbation gradient approximation *Tr. on Automatic Control* p 332-341, 37(3)

[7] Lou D and Weiland S 2018 Parametric model order reduction for large-scale and complex thermal systems *IEEE 2018 European Control Conference* p 2593-2598 June 12-15 2018, Limassol, Cyprus

[8] Arnoldi W E 1951 The principle of minimized iterations in the solution of the matrix eigenvalue problem *Quart. Appl. Math.* P 17–29, Vol 9

[9] Skogestad S and Postlewaite I 2005 Multivariable feedback control – Analysis and design, Chapter 9 *John Wiley & Sons, Inc.*, Chichester, West Sussex, England

[10] Wortelboer P 1994 Frequency-weighted balanced reduction of closed-loop mechanical servo systems: Theory and tools. *Ph.d. dissertation,* Delft University of Technology

[11] Wortelboer P, Steinbuch M and Bosgra O H 1999 Iterative Model and Controller reduction using closed-loop balancing, with application to a compact disc mechanism *Int. J. of Robust and Nonlinear Control*, p 123-142, 9(3)

[12] Merks R 2019 Towards control relevant system design and constrained order controller synthesis: with a thermal control application in immersion lithography *Ph.d. dissertation,* Eindhoven University of Technology